

Improved Density in Aligned Arrays of Single-Walled Carbon Nanotubes by Sequential Chemical Vapor Deposition on Quartz

*By Suck Won Hong and John A. Rogers**

[*] Corresponding author: Prof. J. A. Rogers

Prof. John A. Rogers,

Department of Materials Science and Engineering, Chemistry, Mechanical Science and

Engineering, Electrical and Computer Engineering

Beckman Institute for Advanced Science and Technology, and Frederick Seitz Materials

Research Laboratory

University of Illinois at Urbana-Champaign

Urbana, Illinois 61801 (USA)

E-mail: jrogers@uiuc.edu

Dr. Suck Won Hong,

Department of Materials Science and Engineering

Frederick Seitz Materials Research Laboratory

University of Illinois at Urbana-Champaign

Urbana, Illinois 61801 (USA)

[**] We thank T. Banks for help with processing, using facilities at the Frederick Seitz Materials Research Laboratory. This material is based upon work supported by DARPA.

Keywords: carbon, nanotube, aligned array, chemical vapor deposition (CVD), surface growth, transistor

Guided chemical vapor deposition (CVD) growth of single walled carbon nanotubes on certain crystalline substrates, such as sapphire and quartz, provides an attractive route to linear, horizontally aligned arrays of individual SWNTs.^[1-2] Such configurations, particularly those formed on quartz, are of interest because of their demonstrated ability for wafer-scale integration into devices, including transistors,^[3-4] light emitting diodes,^[5] sensors, photodetectors, and fully integrated systems, such as transistor radios,^[6] logic gates,^[7] and radio frequency oscillators^[8] and devices.^[9] The most well developed strategies use CVD with narrow, patterned lines of catalyst on single crystalline quartz substrates. Detailed experimental and theoretical studies reveal that orientation dependent van der Waals interactions between the SWNTs and the quartz lattice can explain all observations in this system, including growth results for X, Y, Z and ST cuts of crystalline quartz and amorphous quartz.^[10] For ST and AT cuts, the process yields a single, predominant preferred alignment direction in the SWNTs.^[2,11-15] When the catalyst lines are oriented perpendicular to this direction, CVD yields aligned arrays, with exceptionally high levels of perfection in alignment and linearity.^[16-17]

In many applications, increasing the density of such SWNT arrays, as measured by the number of tubes per unit length perpendicular to the alignment direction, improves the properties of the devices that are formed with them. One means to increase the SWNT density involves simply increasing the density (i.e., surface area coverage) of the catalyst particles in each of the catalyst lines. This approach is effective, but only up to some level beyond which the growth tends to yield bundles of SWNTs and multiwalled tubes that involve substantial growth out of the plane of the substrate and in otherwise unaligned configurations. The latter effect arises partly from a decrease in the alignment

forces with increasing diameters of the SWNTs (or bundles of SWNTs). Misaligned SWNTs that grown on the surface can physically block the emergence of aligned SWNTs from the catalyst lines, thereby further frustrating the realization of high densities. Similar phenomena can limit the effectiveness of approaches that optimize the growth conditions to improve the yield of SWNTs from catalyst particles at a fixed density. A different strategy that also involves fixed density relies on reducing the spacing between the lines. Experiments show clearly, however, that this method is ineffective because SWNTs that originate from one catalyst line cannot pass through another catalyst line (See supporting information). This behavior results from the near-surface growth mode observed in these systems, in which even very slight relief, associated with either with misaligned SWNTs or with catalyst particles, can terminate the growth.^[17,18-19] As a result, the SWNT density does not depend strongly on catalyst line separation, provided that this separation is substantially less than the average lengths of the grown SWNTs (e.g., between 200 and 500 μm for typical cases). Given these constraints, although high densities of SWNTs can be obtained over small areas in certain circumstances, they cannot generally be achieved with reproducible, area averaged values much larger than 10 SWNTs μm^{-1} ; typical results are often in the range of 5 SWNTs μm^{-1} .

We report here a simple route to improve the density of SWNTs that avoids limitations described above. The approach relies on multiple, separate CVD growth cycles on a single substrate, as illustrated schematically in Fig. 1. Briefly, the first step involves CVD growth on quartz, using optimized densities of catalyst particles and separations between catalyst lines, as per the discussion above and as reported previously. Next, an additional set of catalyst lines is deposited in regions next to the original ones.

Another cycle of CVD growth yields SWNTs predominantly from the new catalyst lines, thereby increasing the density of the SWNTs in the arrays. The details of each growth process builds on previously reported procedures. In particular, the substrates consist of ST cut quartz wafers (Hoffman Materials INC.) pre-annealed for 8 hrs at 900 °C in air. Photolithography and liftoff define catalyst lines (typical widths 10 μm) that consist of a ~1 Å thick film of iron deposited by electron beam evaporation (Figure 1a). Annealing followed by reduction in hydrogen gas forms catalytic iron particles. The CVD process uses ethanol as a carbon feedstock, with growth in a quartz reaction tube (1 inch diameter) at 925 °C under argon and hydrogen gas flow (Fig. 1b). Next, selective exposure of segments of the SWNT grown in this manner to an oxygen plasma creates lines (typical widths 10 μm) of bare quartz next to the original set of catalyst particles (Fig. 1c). Depositing fresh catalysts in this region (Figure 1d), followed by a second CVD growth yields a new set of aligned SWNTs, thereby increasing the density by roughly 1.5 times for the case illustrated here (Figure 1e). For the second growth, the conditions for annealing and reducing the catalyst must be carefully selected to avoid damaging the pre-existing SWNTs. In particular, flushing the reaction chamber with argon gas helps to eliminate oxygen that would otherwise consume the SWNTs during the annealing step. Likewise, diluted (with argon) levels of hydrogen gas avoid degradation during reduction.

Scanning electron microscope (SEM) and atomic force microscope (AFM) measurements presented in Fig. 2a show typical results from the scheme of Fig. 1. The samples in these cases involve some regions of single growth (i.e., Fig. 1b) and other adjacent regions of double growth (i.e., Fig. 1e). The SEM images are brighter in the

double growth areas (dashed box in yellow, including both 1st and 2nd catalyst lines), resulting from the increased density of SWNTs, compared to the single grown areas (dashed box in blue, including 1st catalyst only). AFM images (insets: 5x5 μm^2) confirm that the densities of SWNTs in the double grown areas are approximately 1.5-2 times higher than in the single grown areas, as expected based on the simple arguments presented previously with additional information in the supplementary materials. Figure 2b shows a case in which the second growth yielded substantially more SWNTs than the first growth, due to slight variability in the process. The densities are, as a result, somewhat better than a typical case, reaching values of 20-30 SWNTs μm^{-1} uniformly over the entire double growth area, with peaks of ~ 45 SWNTs μm^{-1} in certain regions (inset AFM image).

Figure 3a and 3b present SEM images of SWNTs arrays formed by first and second growths using iron catalyst patterned into continuous and dashed line geometries, respectively. These dashed catalyst lines (2nd growth) lie parallel to and equidistant between the continuous catalyst lines (1st growth; Fig. 3b). This layout provides directly adjacent regions composed of areas of single and double growth, suitable for investigation using electrical test structures. The test structures involved pairs of Pd electrodes (45 nm) formed by electron beam evaporation and photolithography and liftoff on both single and double growth areas (inset of Fig. 3c shows the case of double growth), followed by oxygen plasma etching to remove SWNTs not located in the space between the electrodes (Fig 3c and 3d). The widths and separations of the Pd electrodes were 76 μm and 4 μm , respectively. Figure 3e shows an AFM image of SWNTs between two electrodes (top and bottom). Current (I) / voltage (V) characteristics measured in ambient

conditions yield responses like those presented in Fig. 3f. As expected, the current levels measured from devices built with double growth SWNTs are larger, by between 1.5 and 2 times, than the single growth cases, for both positive and negative bias conditions. This outcome is consistent with the corresponding densities of SWNTs obtained from AFM and SEM images (Fig. 2a). Linear fits to these data define effective resistances, R . A histogram that shows the distributions of R values measured from 20 devices in each region appear in Fig. 3g (single growth – black; double growth – red bars).

To demonstrate the utility of multiple growth strategies for devices, we built arrays of top-gated SWNT array based field-effect transistors. Figure 4a shows the schematic side view of such a device. We used a layer of HfO_2 (50 nm) and Au (45 nm) for the gate dielectric and the gate electrode, respectively, on source/drain electrodes of Pd. An optical image of a set of such devices appears in Fig. 4b; oval regions where the HfO_2 was removed by HF provide electrical probing access points to the source and drain electrodes. Figure 4c presents plots of the drain current (I_d) as a function of gate voltage (V_g); forward and reverse sweeps between -3 and 3 V) for a source/drain bias (V_{ds}) of 0.05 V, for devices that use SWNT arrays formed by single (density, $D = \sim 4\text{-}7$ SWNTs μm^{-1}) and double ($D = \sim 7\text{-}15$ SWNTs μm^{-1}) growth. In both cases, the channel length, L , is 4 μm and the channel width, W , is 76 μm . The histograms in Fig. 4d summarize the results of similar measurements for 20 devices of each type (single growth – black; double growth – red bars). Metrics for comparison include currents measured in the p -channel ‘on state’ (i.e., $V_g = -3$ V), the ‘off state’ (i.e., V_g set to realize the minimum I_d , typically between 0 and 0.5 V) and the n -channel ‘on state’ (i.e., $V_g = 3$ V). To within experimental uncertainties, these results are consistent with microscopy and two terminal

device measurements. Ignoring the effects of contacts, the resistivities (i.e., the resistances per unit length) per tube for the metallic tubes can be estimated from the resistance at the minimum current values in transfer curves such as those shown in Fig. 4c. For both the single and double growth areas, the average resistivity is $\sim 20\text{-}50 \text{ k}\Omega \mu\text{m}^{-1}$. This number and the current in the on state can be used to estimate the resistivities for the semiconducting tubes; the result is $\sim 60\text{-}90 \text{ k}\Omega \mu\text{m}^{-1}$. All of these results are consistent with previous reports of SWNT arrays grown on quartz.^[21]

From the above results, the linear regime mobilities can be calculated, using the peak transconductance for single and double growth devices at a source/drain bias (V_{ds}) of 0.05 V. Here, we define the effective field-effect mobility, μ as

$$\mu = \frac{L}{V_d C_w W} \cdot \frac{dI_d}{dV_g} \quad (1)$$

where C_w is the specific capacitance per unit area for the electrostatic coupling of the aligned array of SWNTs to the planar gate,^[16,20] according to the following expression:

$$C_w = \frac{D}{\left[C_Q^{-1} + \frac{1}{2\pi\epsilon_0\epsilon_s} \cdot \log \left[\frac{\sinh(2\pi tD)}{\pi rD} \right] \right]} \quad (2)$$

where D is the density of the arrays of SWNTs per unit width, C_Q is the quantum capacitance, t is the distance to the gate electrode, ϵ_0 is the permittivity of free space, ϵ_s is the dielectric constant of the gate dielectric, and r is the SWNT radius. For the purpose of calculation, we consider only the semiconducting tubes in our estimate of D because the corresponding modulation by the gate originates primarily from such tubes; we assume that the ratio of metallic to semiconducting nanotubes is 1:2.^[16] For the dielectric

constant of the hafnium oxide and the quantum capacitance of nanotubes, we used 10 and $\sim 3.2 \times 10^{-10} \text{ F m}^{-1}$, respectively.

The calculated effective mobilities in the double growth areas for 20 devices of each type show values as high as $\sim 800 \text{ cm}^2 \text{ V}^{-1} \text{ s}^{-1}$ (median $\sim 650 \text{ cm}^2 \text{ V}^{-1} \text{ s}^{-1}$) and $\sim 560 \text{ cm}^2 \text{ V}^{-1} \text{ s}^{-1}$ (median $\sim 400 \text{ cm}^2 \text{ V}^{-1} \text{ s}^{-1}$) for the *p*-channel mode and the *n*-channel mode, respectively. Otherwise, the values for the single growth devices are typically $\sim 633 \text{ cm}^2 \text{ V}^{-1} \text{ s}^{-1}$ (*p*-channel mode) and $\sim 320 \text{ cm}^2 \text{ V}^{-1} \text{ s}^{-1}$ (*n*-channel mode). Due to the relatively large hysteresis in these devices, the extracted mobilities depend on direction of the sweep in the gate voltage. The above calculations correspond to sweeps with increasing gate voltage. Similar analysis for the opposite sweep yields values that are lower by $\sim 20 \%$ for the *p*-channel mode. In addition, we do not attempt to account for effects of contact resistances between the source/drain electrodes and the semiconducting tubes. Estimates of these resistances,^[21] suggest that the mobilities would be improved by $\sim 20 \%$ by explicitly including them in the analysis. Generally, the values that we observe here are similar to those reported previously in array devices.

In conclusion, this paper presents a simple strategy for doubling the density of horizontally aligned arrays of SWNTs on quartz substrate. Detailed characterization of the tubes by AFM, SEM and electrical measurements on two and three terminal devices reveal the key characteristics of the process and the properties of the arrays. The resulting improvement has direct beneficial effect on devices made using the tubes. This strategy is compatible with various optimized single growth techniques described recently for quartz[CITE REFERENCES TO LIU, BURKE, ZHOU AND ANY OTHERS] In principle, this process can be extended to triple, quadruple, quintuple

growths, and beyond. Due to the arithmetic increase in density with each growth, however, the percentage increases in the density diminish with multiple cycles. For example, double growth increases the density by up to two times compared to single growth. Triple growth only yields an increase of 1.5 times compared to double growth. Quadruple growth yields an increase of only 1.3 times compared to triple growth, and so on. One strategy around such limitation is to combine double or triple growth arrays with multiple transfer printing procedures to multiply the densities. Such approaches could realistically yield densities 20 times higher than those associated with the usual, single growth strategy, with the clear potential to realize reproducible densities in the range of 100 SWNTs μm^{-1} .

Experimental

Synthesis of highly dense aligned SWNTs arrays: ST-cut single crystal quartz substrates (Hoffman Materials Inc.) were thermally annealed at 900 °C for 8 hrs. Iron catalyst lines consisted of thin films (1-5Å) deposited by electron beam evaporation (Temescal BJD1800) and patterned by photolithography (AZ 5214) and lift-off. Heating the substrate prepared in this fashion at 900 °C for 1 hr in quartz reaction chamber oxidized the catalyst. After cooling the substrate to room temperature, heating to 925 °C under hydrogen gas flow with 350 sccm for 10 min fully reduced the catalyst. Chemical vapor deposition (CVD) growth performed for 20 min with a flow of argon (20 sccm) and hydrogen (20 sccm) introduced through an ethanol bubbler at 925 °C, yielded aligned arrays of SWNTs. Before CVD for regrowth, exposure to oxygen plasma for 5 min through a patterned layer of photoresist removed certain segments of the existing SWNTs, thereby exposing the native quartz surface in line geometries next to and parallel with the first set of catalyst lines. Next, a new layer of iron was deposited in these etched regions. Annealing was performed in this case after purging the chamber with argon gas (1500 sccm) for 20 min and under a continuous flow of argon (500 sccm). The reduction used a flow of hydrogen (200 sccm) diluted by argon (50 sccm). The same ethanol CVD growth process was then used.

Electrical measurement: Two terminal devices and transistor measurements were carried out in air using a semiconductor parameter analyzer (Agilent 4156A). Pd contact pads were used in both cases, in layouts that involved removal of SWNTs by oxygen plasma etching in all regions except between pairs of electrodes. For the transistors, the gate dielectric layer (~49 nm) of HfO₂ was deposited by electron beam evaporation

followed by atomic layer deposition (1.5 nm) over the entire substrate. A gate electrode of Au (45 nm) was deposited on top of this dielectric. Etching away the HfO₂ in selected regions opened bare regions of Pd for probing the source and drain electrodes.

Figure Captions

Figure 1. Schematic illustration of the procedures for multiple CVD growth of aligned arrays of SWNTs on quartz. a) The process begins with lithographically patterned iron catalyst lines on annealed quartz. b) CVD growth yields SWNTs that are horizontally aligned on the surface of the quartz, in a direction orthogonal to the catalyst lines. c-d) Patterned removal of SWNTs in narrow lines parallel and next to the iron catalyst regions followed by deposition and annealing of iron forms a new collection of catalyst particles. e) CVD growth of SWNTs from these new iron catalyst lines creates additional aligned SWNTs, thereby increasing the density. For clarity of illustration, the diagrams here show the SWNTs that result from the first and second growth steps in blue and red, respectively. Multiple cycles of this process are possible.

Figure 2. SEM and AFM images of single and double growths of SWNTs on a quartz substrate. a) The 2nd catalyst lines are adjacent and parallel to the 1st catalyst lines. The brighter contrast in the double growth areas (dashed box in yellow) results from a higher density of aligned SWNTs compared to the single grown area (dashed box in blue). AFM images (insets: $5 \times 5 \mu\text{m}^2$) confirm that the density of SWNTs in the double growth areas is between 1.5 and 2 times that in the single grown area. The images shown here represent a typical case. b) Images of a substrate, similar to that shown in (a), but with SWNTs at densities that are better than typical. Here, the densities are 20-30 SWNTs μm^{-1} , uniformly over the entire double growth area, with peak values that approach ~ 45 SWNTs μm^{-1} .

Figure 3. a-b) SEM images of SWNTs after a double growth process, where the first and second growths involved iron catalyst patterned into continuous and dashed line geometries, respectively. The dashed lines are parallel to and equidistant between the continuous lines. This layout provides adjacent areas that have SWNTs at single and double growth densities, for ease of comparing the collective electrical properties of the arrays. c-d) Pairs of electrodes (Pd, 45 nm) were patterned on top of single growth and double growth areas (inset). The devices were then isolated by etching away the SWNTs not located in the space between the electrodes. The widths and spacings of the electrodes were 76 μm and 4 μm , respectively. e) AFM image of SWNTs between two electrodes. f) Current-voltage characteristics for representative devices. Linear fits to these data define effective resistances. g) Histogram of the resistance between pairs of electrodes for the single growth and regrowth regions (20 devices in each region were measured).

Figure 4. a) Schematic side view of a top-gated SWNT array transistor that uses a layer of HfO_2 for the gate dielectric, Au for the gate electrode and Pd for source and drain electrodes. b) Optical image of a set of such devices. Oval regions where the HfO_2 was removed provide electrical contact points to the source and drain electrodes. c) Drain current (I_d) as a function of gate voltage (V_g) for a source/drain bias (V_{ds}) of 0.05 V, for a transistor (channel length, $L = 4 \mu\text{m}$; channel width, $W = 76 \mu\text{m}$) that incorporates aligned arrays of SWNTs from single growth (density, $D = \sim 4\text{-}7 \text{ SWNTs } \mu\text{m}^{-1}$) and from regrowth ($D = \sim 7\text{-}15 \text{ SWNTs } \mu\text{m}^{-1}$). The open and solid circles indicate the sweep direction of gate voltage (solid – sweep up; open – sweep down). d) Histograms of

current measured in the p -channel ‘on state’ (i.e. $V_g = -3$ V), the ‘off state’ (i.e. V_g set to realize the minimum I_d , typically between 0 and 0.5 V) and the n -channel ‘on state’ (i.e. $V_g = 3$ V) for transistors built in regions of single growth (black bars) and regrowth (red bars). e) Histograms of mobilities calculated from a series of peak transconductance in the p -channel and the n -channel for each 20 devices (single growth – black; double growth – red bars).

References

- [1] A. Ismach, L. Segev, E. Wachtel and E. Joselevich, *Angew. Chem., Int. Ed.* **2004**, 43, 6140.
- [2] C. Kocabas, S. H. Hur, A. Gaur, M. A. Meitl, M. Shim, J. A. Rogers, *Small* **2005**, 1, 1110.
- [3] S. Kim, S. Ju, J. H. Back, Y. Xuan, P. D. Ye, M. Shim, D. B. Janes, S. Mohammadi, *Adv. Mater.* **2009**, 21, 564.
- [4] S. Jeon, C. Lee, J. Tang, J. Hone, C. Nuckolls, *Nano Res.* **2008**, 1, 427.
- [5] J. Zaumseil, X. Ho, J. R. Guest, G. P. Wiederrecht, J. A. Rogers, *ACS Nano* **2009**, 8, 2225.
- [6] C. Kocabas, H. S. Kim, T. Banks, J. A. Rogers, A. A. Pesetski, J. E. Baumgardner, S. V. Krishnaswamy, H. Zhang, *Proc. Natl. Acad. Sci. U. S. A.* **2008**, 105, 1405.
- [7] K. Ryu, A. Badmaev, C. Wang, A. Lin, N. Patil, L. Gomez, A. Kumar, S. Mitra, H.-S. P. Wong, C. Zhou, *Nano Lett.* **2009**, 9, 189.
- [8] A. A. Pesetski, J. E. Baumgardner, S. V. Krishnaswamy, H. Zhang, J. D. Adam, C. Kocabas, T. Banks, J. A. Rogers, *Appl. Phys. Lett.* **2008**, 93, 123506.
- [9] C. Kocabas, S. Dunham, Q. Cao, K. Cimino, X. Ho, H.-S. Kim, D. Dawson, J. Payne, M. Stuenkel, H. Zhang, T. Banks, M. Feng, S. V. Rotkin, J. A. Rogers *Nano Lett.* **2009**, 9, 1937.
- [10] J. Xiao, S. Dunham, P. Liu, Y. Zhang, C. Kocabas, L. Moh, Y. Huang, K.-C. Hwang, C. Lu, W. Huang, J. A. Rogers, **2009 Submitted**
- [11] C. Kocabas, N. Pimparkar, O. Yesilyurt, S. J. Kang, M. A. Alam, J. A. Rogers, *Nano Lett.* **2007**, 7, 1195.

- [12] L. Ding, D. Yuan, J. Liu, *J. Am. Chem. Soc.* **2008**, 130, 5428.
- [13] W. Zhou, C. Rutherglen, P. J. Burke, *Nano Res.* **2008**, 1, 158.
- [14] B. Li, C. F. Goh, X. Zhou, G. Lu, H. Tantang, Y. Chen, C. Xue, F. Y. C. Boey, H. Zhang, *Adv. Mater.* **2009**, 20, 4873.
- [15] B. Zhang, G. Hong, B. Peng, J. Zhang, W. Choi, J. M. Kim, J.-Y. Choi, Z. Liu, *J. Phys. Chem. C*, **2009**, 113, 5341.
- [16] S. J. Kang, C. Kocabas, T. Ozel, M. Shim, N. Pimparkar, M. A. Alam, S. V. Rotkin, J. A. Rogers, *Nat. Nanotechnol.* **2007**, 2, 230.
- [17] C. Kocabas, M. Shim, J. A. Rogers, *J. Am. Chem. Soc.* **2006**, 128, 4540.
- [18] S. Huang, B. Maynor, X. Cai, J. Liu, *Adv. Mater.* **2003**, 15, 1695
- [19] B. Li, X. Cao, X. Huang, G. Lu, Y. Huang, C. H. Goh, F. Y. C. Boey H. Zhang, *Small* **2009**, 5, 2061
- [20] Q. Cao, M. Xia, C. Kocabas, M. Shim, J. A. Rogers, S. V. Rotkin, *Appl. Phys. Lett.* **2007**, 90, 023516.
- [21] X. Ho, L. Ye, S. V. Rotkin, J. A. Rogers, **2009 Submitted**

Figure 1.

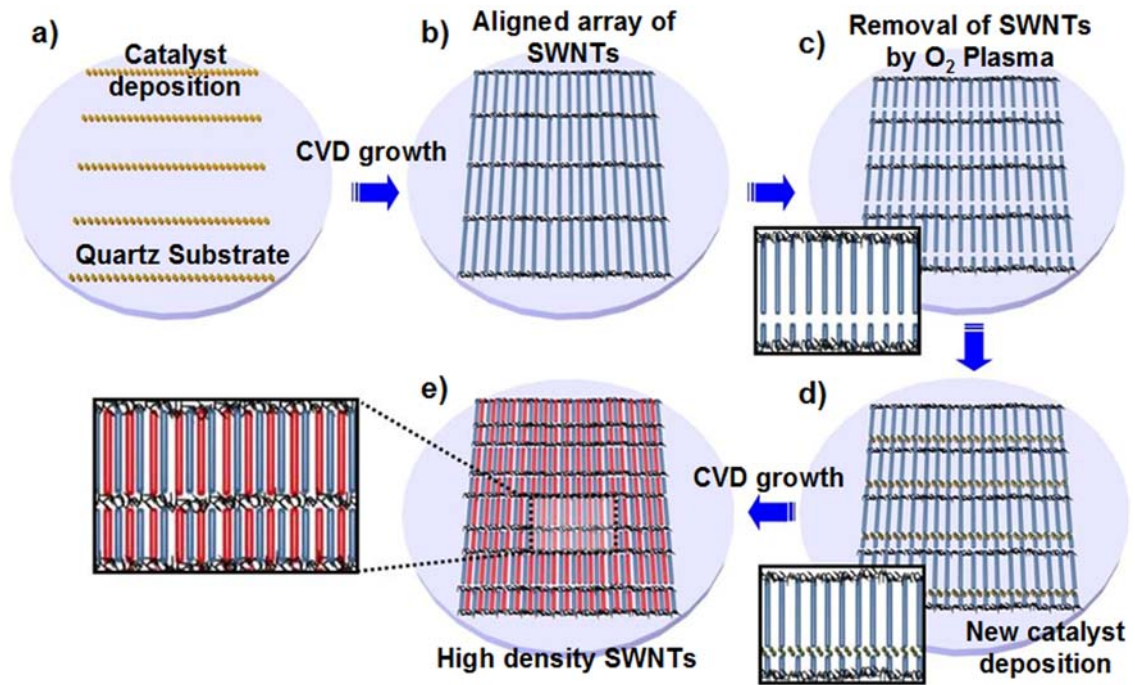


Figure 2.

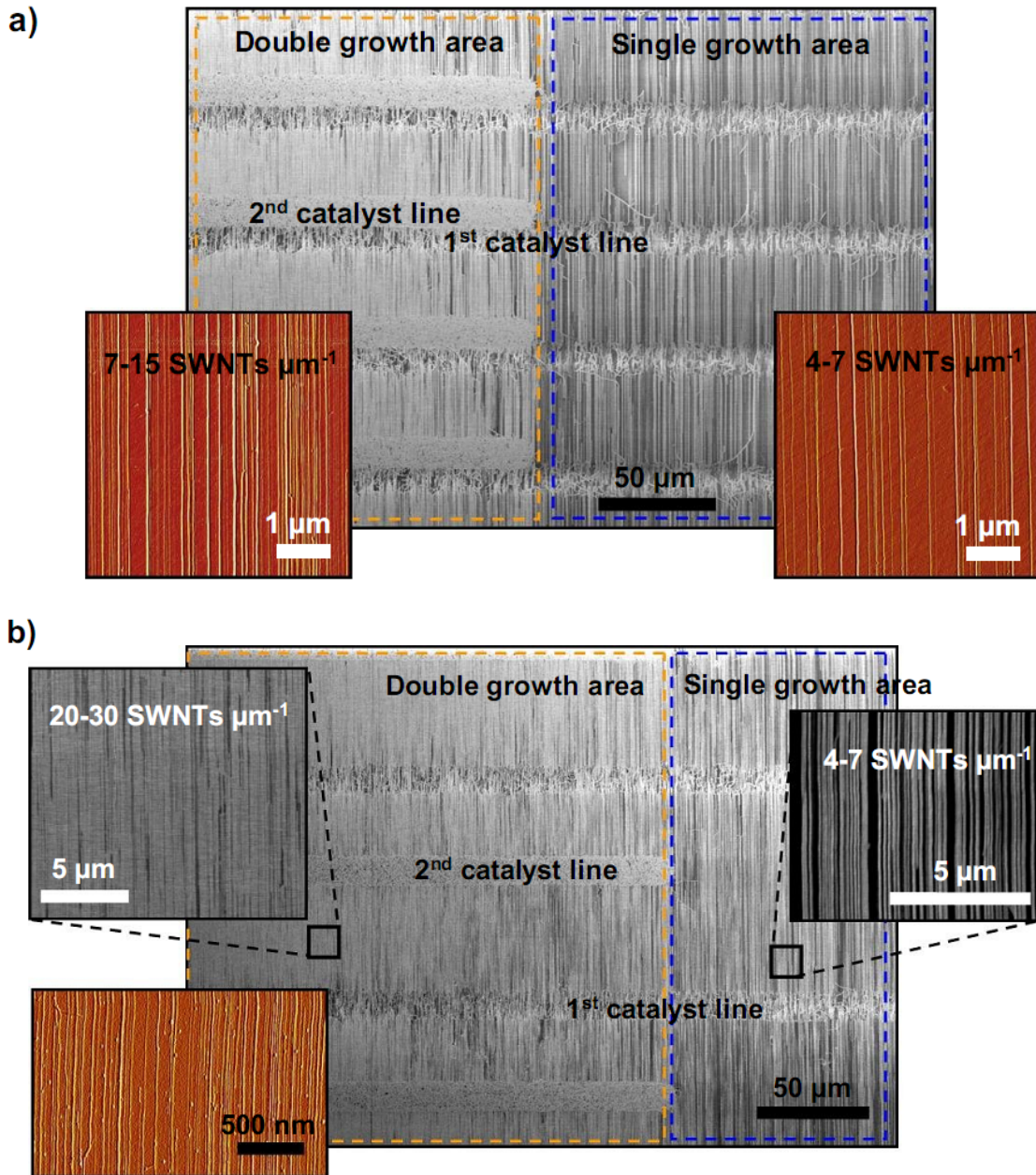


Figure 3.

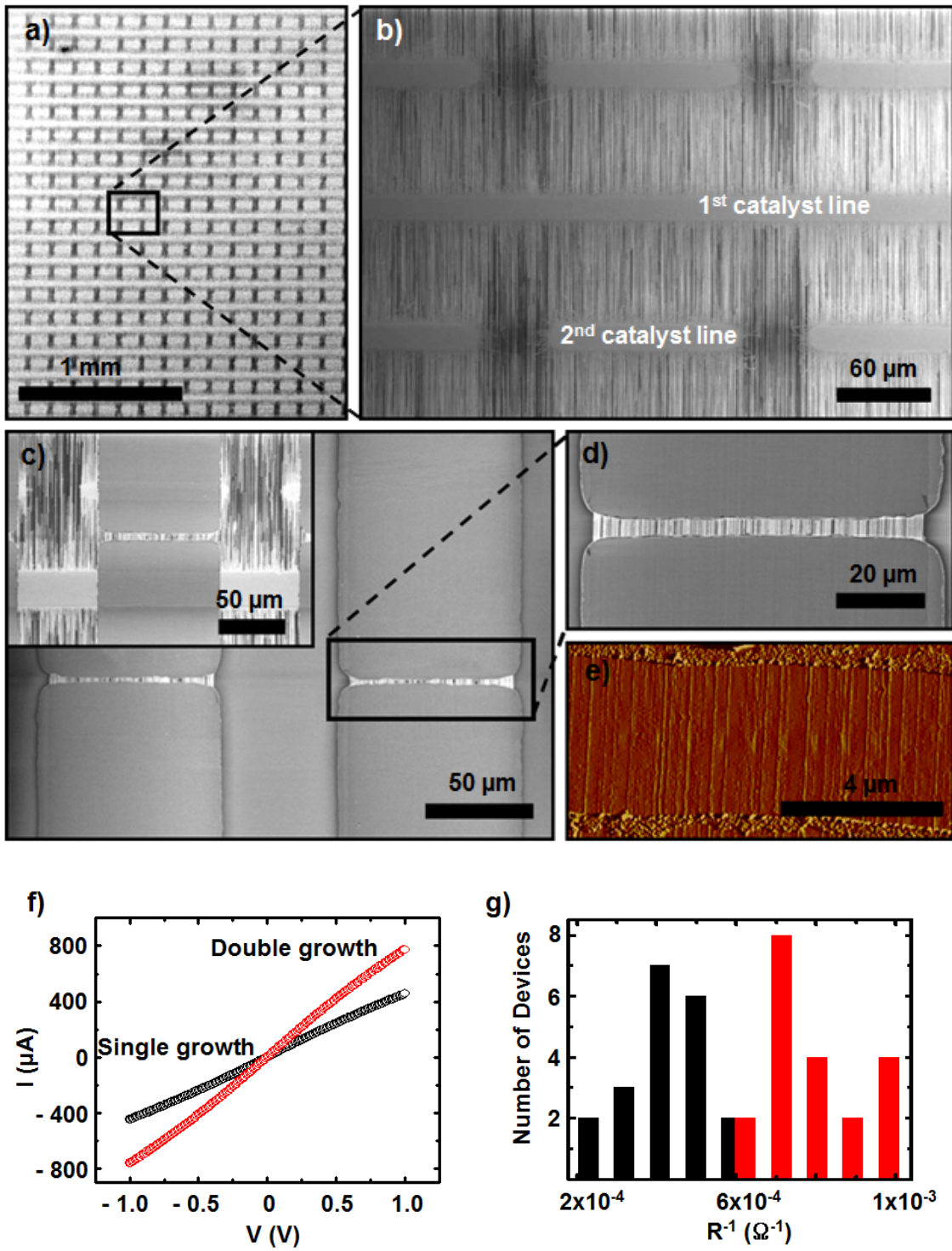
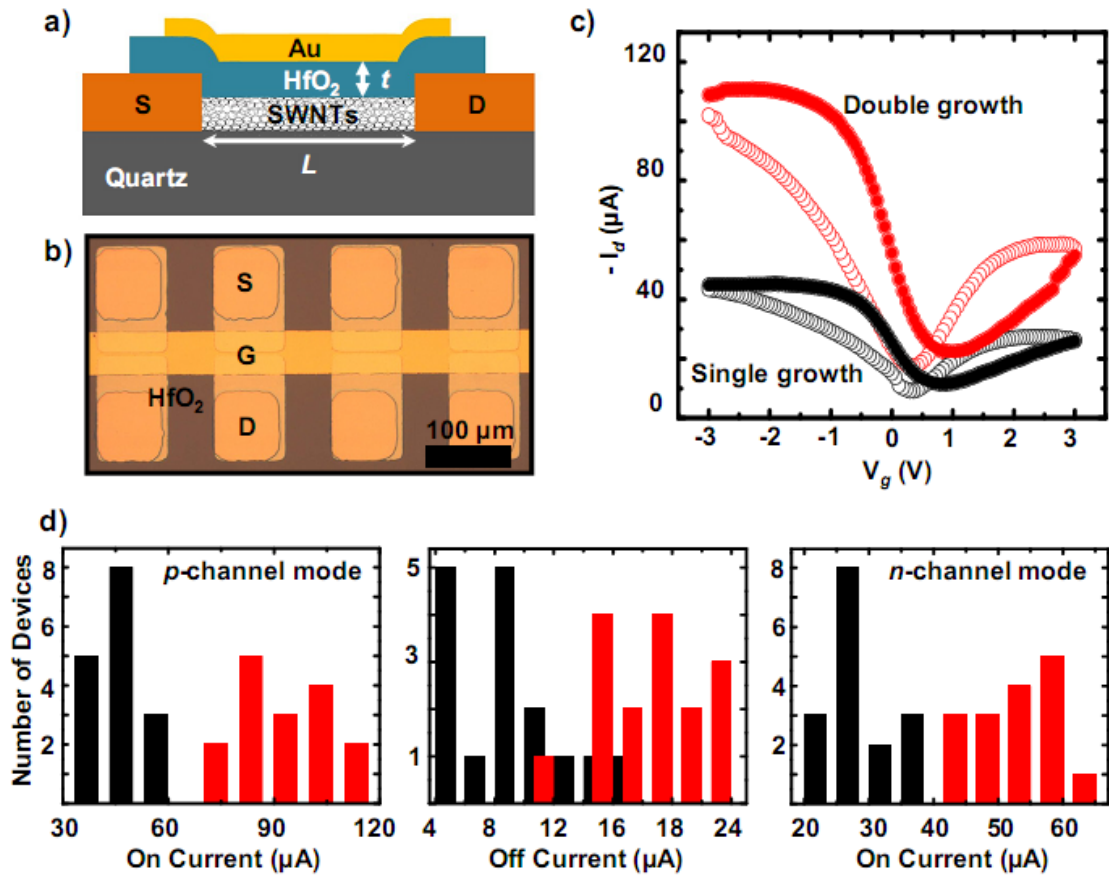


Figure 4.



Improved Density in Aligned Arrays of Single-Walled Carbon Nanotubes by Sequential Chemical Vapor Deposition on Quartz

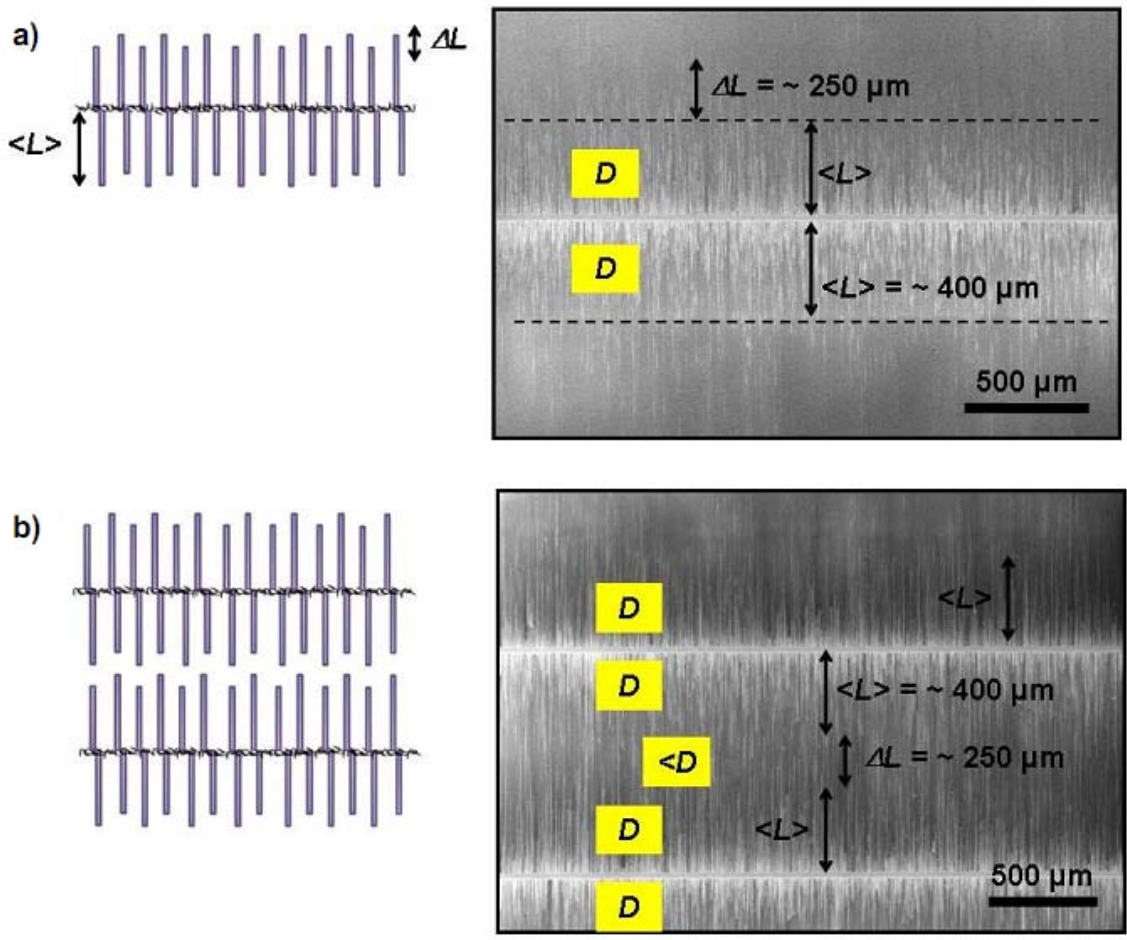
*By Suck Won Hong and John A. Rogers**

Supporting Information

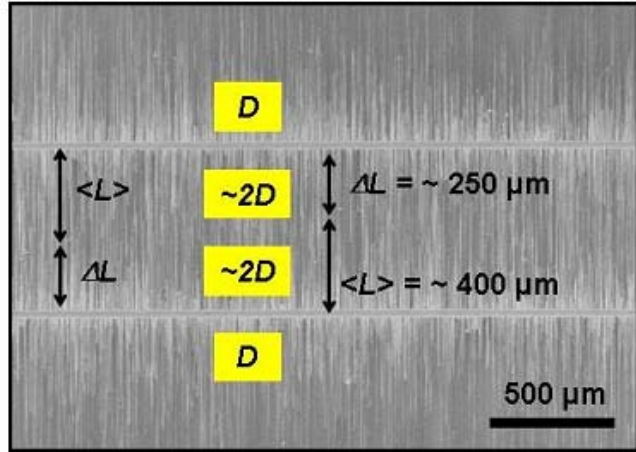
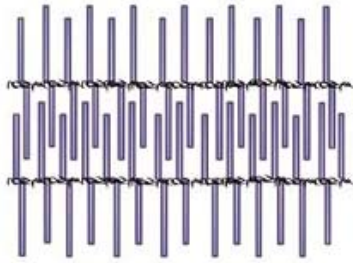
The regrowth approach can be rationalized according to the following view of the process, as illustrated schematically and demonstrated experimentally in Fig. S1. We define the average density of SWNTs as D , the uniform length of SWNTs as $\langle L \rangle$, and a characteristic measure of the variation in this length as ΔL , all determined experimentally from examination of SWNTs that grow from a single line of catalyst with an orientation perpendicular to the preferred growth direction (Figure S1a). For typical cases illustrated here, $D = 1\text{-}3 \text{ SWNTs } \mu\text{m}^{-1}$, $\langle L \rangle = \sim 400 \text{ } \mu\text{m}$, and $\Delta L = \sim 250 \text{ } \mu\text{m}$, respectively. As the separation between a pair of parallel, catalyst lines (Figure S1b, S1c, and Figure S1d) decreases, the density of SWNTs between two catalyst lines was gradually increases as the separation approaches $\sim \langle L \rangle$ (Figure S1d), as might be expected. In other words, as the separation moves from values larger than $\langle L \rangle$ (Figure S1b and S1c) to comparable to or smaller than $\langle L \rangle$ (Figure S1d), the uniformity and density of SWNTs (i.e., $2D$) are improved (Figure S1d). Once the separation is significantly below $\langle L \rangle - \Delta L$, the density no longer depends strongly on separation. The density of SWNTs that emerge from the a given catalyst line is independent of proximity to other catalyst lines. In addition, growing SWNT from one catalyst line cannot penetrate another catalyst line.

Based on this view of the process, the double growth strategy achieves densities in SWNT arrays that no arrangement of catalyst lines in a single growth process can achieve.

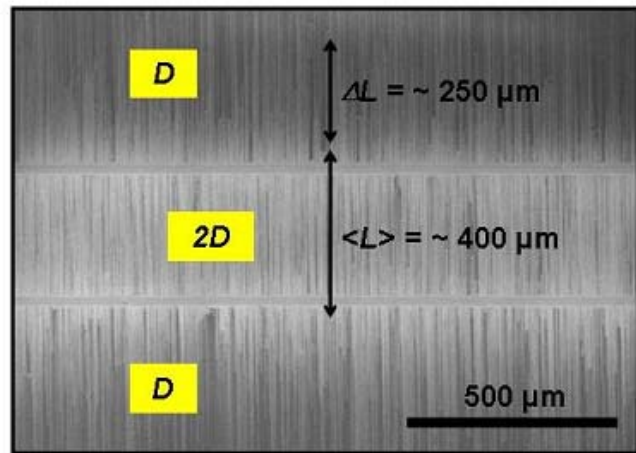
(Figure 1e and Figure 2).



c)



d)



e)

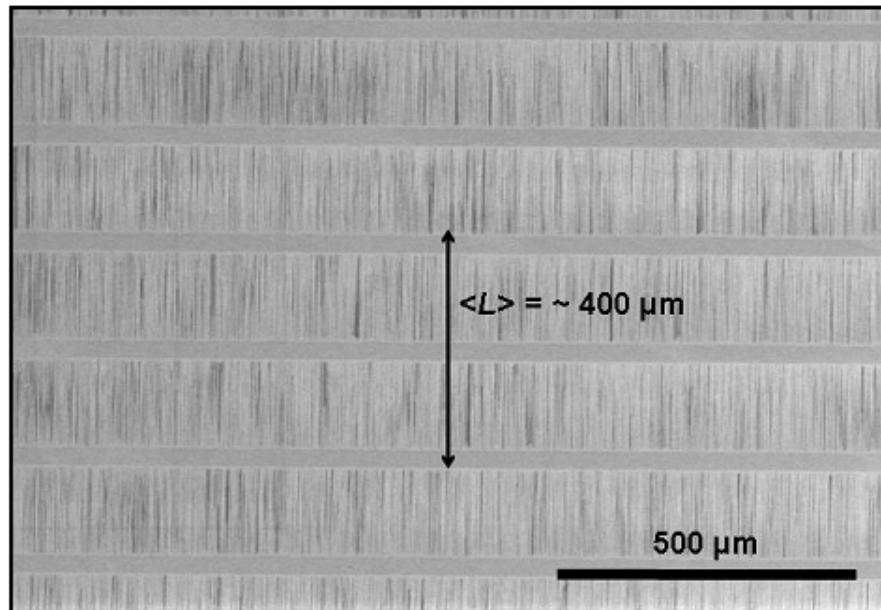


Figure S1. Proposed model for aligned SWNTs growth system and experimental results.

a) Average density of SWNTs, D , the uniform length of SWNTs, $\langle L \rangle$, and the variant of a length of SWNTs, ΔL was defined from the one isolated catalyst line. b) Catalyst lines separated by a distance bigger than $\langle L \rangle$. c) Catalyst lines separated by a distance smaller than $\langle L \rangle$. d) Catalyst lines separated by around distance $\langle L \rangle$. e) Catalyst lines separated by a distance much smaller than $\langle L \rangle$.